Colloidal Ag@Pt Core–Shell Nanoparticles for the Catalytic Reduction of Nitrophenol

Yinan Fan, Caroline Salzemann, Benoit Tremblay, Adrien Girard, Alexa Courty

Colloidal Ag@Pt Core-shell Nanoparticles for the Catalytic Reduction of Nitrophenol.

Yinan Fan[†], Caroline Salzemann[†], Benoit Tremblay[†], Adrien Girard*[†] and Alexa Courty*[†]

[†]Sorbonne Université, MONARIS, CNRS-UMR 8233, 75005 Paris, France

KEYWORDS: bimetallic nanoparticles, core-shell nanoparticles, nitrophenol, plasmonic, catalysis

Abstract.

Bimetallic nanoparticles (NPs) composed of two metal elements have attracted much interest due to the possibility to synergistically enhance the catalytic performance of nanocatalysts. In this context, we have recently reported the seed mediated growth of bimetallic core-shell NPs combining a plasmonic metal Ag as a core and a catalytic metal Pt as a shell with a fine control of the core size and shell thickness. Here, we report a detailed study of the catalytic properties of our Ag@Pt core-shell NPs through a model reaction of reduction of 4-nitrophenol (4-NP) in 4-aminophenol (4-AP) in the presence of $NaBH_4$, where the Pt shell thickness can be tuned from 1 to 6 atomic layers by adjusting the ratio of the Pt precursor to Ag seed concentration. First, we optimized the catalytic performances of pure Ag NPs by showing the role played by protons. We showed that the addition of an aqueous HCl or H_2SO_4 solution improves the catalytic conversion rate due to the addition of H^+. Furthermore, we showed that under light irradiation the presence of halide increases the catalytic efficiency of the Ag NPs by a photo-recycling of Ag and the generation of hot electrons. We then evidenced that the bimetallic system is more catalytically active than its monometallic counterparts, highlighting how the synergy between the two metals crucially depends on both the thickness of the Pt shell and the size of the Ag core. The best conditions were found with 4 Pt atomic layers, which is

attributed to a favorable electronic coupling between Pt shell and Ag core. Nevertheless, the effect of the irradiation on the catalytic activity of Ag@Pt NPs remains moderate probably due to localized surface plasmon resonance damping by the Pt shell. Finally, the Ag@Pt NPs showed a good stability and could be reused after running 3 recycling, thus opening perspectives for the rational design of core-shell nanocatalysts with controlled shell morphologies.

1. Introduction

Bimetallic nanoparticles (NPs) have aroused much interest lately due to the possibility to combine two metals to obtain improved properties compared to the sum of the individual parts.[1] This has been particularly acknowledged by both the catalytic and plasmonic communities, which take benefit of both a noble metal and a catalytic metals to engineer new nanocatalysts with enhanced properties.[2] Noble metals such as Au, Ag or Cu are catalytically active for only a reduced number of reactions but support plasmon resonances in the visible range, while catalytic metals such as Pt or Pd don't support plasmonic resonances in the visible range but are catalytically active for a broader range of reactions. Combining plasmonic excitations and catalytic activity of both metals is therefore very attractive for improving catalytic properties compared to monometallic nanoparticles.[3]

The excitation of noble metal NPs at their localized surface plasmon resonance (LSPR) can impact catalysis reactions via several mechanisms[4–7]. First the optical power absorbed by an irradiated NP is restituted to its local environment in the form of heat on the picosecond scale, which has great promises to overcome the limitations of traditional resistive heating in order to reduce the activation barrier of various reactions steps (fuel cost and increased byproduct formation).[4] Secondly, the electronic oscillation induced by

the illumination acts as an electromagnetic dipole, concentrating light at the NP surface. The large increase of available photons can be used to drive locally photochemical reactions with a much higher rate. Last, hot electron generation at energy levels between E_f and E_f - hν (where E_f is the Fermi energy of the metal and hν the photon energy) can be used to inject energetic charge carriers (electrons or holes) into nearby acceptor molecules, thereby driving chemical reactions and promoting specific reaction pathways for product selectivity.[5,9] This effect is primarily located at so-called "hotspots" within coupled nanostructures. Bimetallic nanocatalysts ideally combine the properties of both the plasmonic and the catalytic metal, and have been evidenced to show better product selectivity[10,11] as well as improved reaction rates[12,13] and optical sensivity.[14]

Bimetallic nanocatalysts can be engineered in different configurations, namely the antenna - reactor, alloy and core-shell geometries, which have their own intermetallic interactions governing the catalytic response.[15] Unlike the antenna reactor geometry, based on optical coupling between the two metals, the core-shell geometry combines both optical and electronic interactions with distinct interface between the two metals.[16] This is most often realized with a plasmonic core and a thin catalytic shell, and this type of nanoreactors have been made mainly from wet chemistry. The direct interface between the two metals changes their electronic structure compared to the monometallic counterparts, and can up-shift or down-shift the position of the d-band center of the shell due to mechanical strain effects, thereby influencing how molecular reactants adsorb on the nanocatalysts and thus the reactivity.[17] On the other hand, the plasmonic core is also affected by the capping by a catalytic shell, with a LSPR shifted and all the more damped the thicker the catalytic shell.[18]

Core-shell bimetallic nanocatalysts based on the association of a plasmonic core and a catalytic shell have been shown to exhibit higher activity compared to both the

monometallic and alloy counter parts[19,20], and exhibit interesting possibilities for increased efficiency. Within this context, we recently published the synthesis of core-shell Ag@Pt NPs via a seeded mediated growth process with a good control of both the core size distribution (≤10%) and the Pt shell thickness (from 1 to 6 atomic layers).[18] We have investigated both experimentally and theoretically their optical behavior and we have evidenced a damping of the LSPR from the first Pt atomic layer surrounding the Ag core. Furthermore, preliminary tests showed that Ag@Pt core-shell NPs had an increased catalytic activity compared to their monometallic counterparts for the reduction of 4-nitrophenol (4-NP) to 4-aminophenol (4-AP) by sodium borohydride ($NaHB_4$) in aqueous phase.

ln this article, we report a thorough investigation of the catalytic properties of our Ag@Pt core-shell NPs with low structural dispersion, controlled core size and shell thickness. We revisited the model reaction of the 4-NP to 4-AP reduction with pure Ag NPs and investigated how acidic conditions can improve the catalytic rate of dispersed Ag NPs in solution through an additional proton supply. Furthermore, we explored how light irradiation and the presence of halide impacts their catalytic efficiency. Then, we have finely characterized the dependence of the catalytic activity with the shell thickness over a 0 - 6 Pt layer range, and identified an optimal number of covering layers for which the best synergy could be observed.. Finally, we addressed the recyclability of our NPs, which showed a good stability after several recycling.

1. Materials and methods

Chemical. Commercial reagents were used without further purification and stored in a glovebox to avoid any traces of moisture or air contamination. Silver nitrate, dioctyl ether, oleic acid (90%), chloroform (≥99%) and $Pt(acac)_2$, were purchased from Sigma-

Aldrich. Oleylamine (80-90%) was bought from ACROS Organics.

Synthesis of Ag and Ag@Pt NPs. The Ag and Ag@Pt NPs with 1-6 Pt atomic layers were synthesized and characterized according to a previously published protocol.[18] Briefly, spherical Ag NPs of controlled size were synthesized by a chemical route in N_2 atmosphere in which $AgNO_3$ in the presence of oleylamine (OLA) transforms to Ag(0) NPs, whose sizes (between 8 and 14 nm in diameter) and size distribution (lower than 10%) are controlled by the reaction time, heating ramp and reaction temperature. Then, Ag@Pt NPs were synthesized via a seed-mediated growth process in which the Ag NPs are used as seeds in presence of a Pt precursor, $Pt(acac)_2$. The Pt shell thickness is controlled by adjusting the concentration ratio between the Pt precursor and the silver seed. The composition and structural analyses were conducted as detailed in our prior publication, employing EELS mapping coupled with STEM HAADF, along with UV-visible spectroscopy complemented by DDA calculations[18]. These techniques robustly substantiated the core-shell architecture in the Ag@Pt nanoparticles, allowing for precise determination of the shell thickness.

TEM imaging. The TEM images were obtained with a JEOL JEM1011 100 kV. The samples for TEM imaging were prepared by putting droplets of a dilute solution on a carbon-coated copper grid.

***UV-Visible Spectroscopies*.** In the range of 300 to 700 nm UV-visible absorption spectra were acquired from all samples with a VARlAN Cary 5000 UV-vis-near-infrared (UV-vis-NIR) spectrometer. For the measurements 4 mL disposable cuvettes (quartz) with a path length of 1 cm were used.

Catalytic Reaction. All reactions were carried out in a 4 mL quartz optical cuvette (lenght=1cm) at atmospheric pressure with temperature control achieved by a water flow, and light irradiation via optical fiber injection, see experimental setup Fig S1. At specific

temperature (20 and 30°C), reagents were added in the following sequence: 3480 µl of 4-NP aqueous solution (C_{NPs}= 0.17 mM), 400 µL of cooled 0.4 M $NaBH_4$ solution (approximately 5°C) to prevent hydrolysis and 20 µl of NP solution. Subsequently, the solution was manually stirred for 30 seconds to ensure homogeneity. The catalytic conversion of 4-NP was analyzed using UV-Vis spectroscopy with background correction performed with deionized water as a reference. For Clarification, the concentrations of Ag and Ag@Pt NPs were precisely controlled. We thus adjusted the concentration in NPs in order to keep the same volume of addition (20 µL) and the same total surface area for each NP solution equal to 7.34 10^{18} nm^2 L^{-1}. The total surface area (S_{Tot}) for a given colloidal solution is defined in the following equation:

$S_{Tot}= N_a$ x C_{NPs} x S (equation 1)

where C_{NPs} is the concentration of NPs, S is the surface area per spherical NP of diameter D, and N_a is the Avogadro constant.

Furthermore, we supposed that the concentration of NPs in solution doesn't change after water transfer since all the particles precipitate after addition of mercaptosuccinic acid (MSA and the whole precipitate is redispersed in water). ***Recyclability:*** After reaction cycle, the catalyst was reused by adding new nitrophenol for a consecutive run under the same reaction condition (temperature and Pressure).

2. Results and discussion

The synthesis of Ag and Ag@Pt NPs with 1-6 Pt atomic layers followed a previously published protocol.[18] In brief, spherical Ag NPs of controlled size were generated through a high-temperature process, where $AgNO_3$, in the presence of oleylamine, transforms into Ag(0) NPs, with sizes determined by reaction time, heating ramp, and temperature. Subsequently, Ag@Pt NPs were synthesized using a seed-mediated growth process, employing Ag NPs as seeds and a Pt precursor ($Pt(acac)_2$). The two-step synthesis

process is depicted in Fig. 1. The Pt shell thickness was controlled by adjusting the concentration ratio between the Pt precursor and the silver seed, with an optimal Pt thickness of 1-6 layers selected. Representative TEM images of the resulting Ag NPs and Ag@Pt NPs are presented in Fig. 1. Ag@Pt NPs exhibit surface irregularities consistent with Pt layer overgrowth on the Ag core.

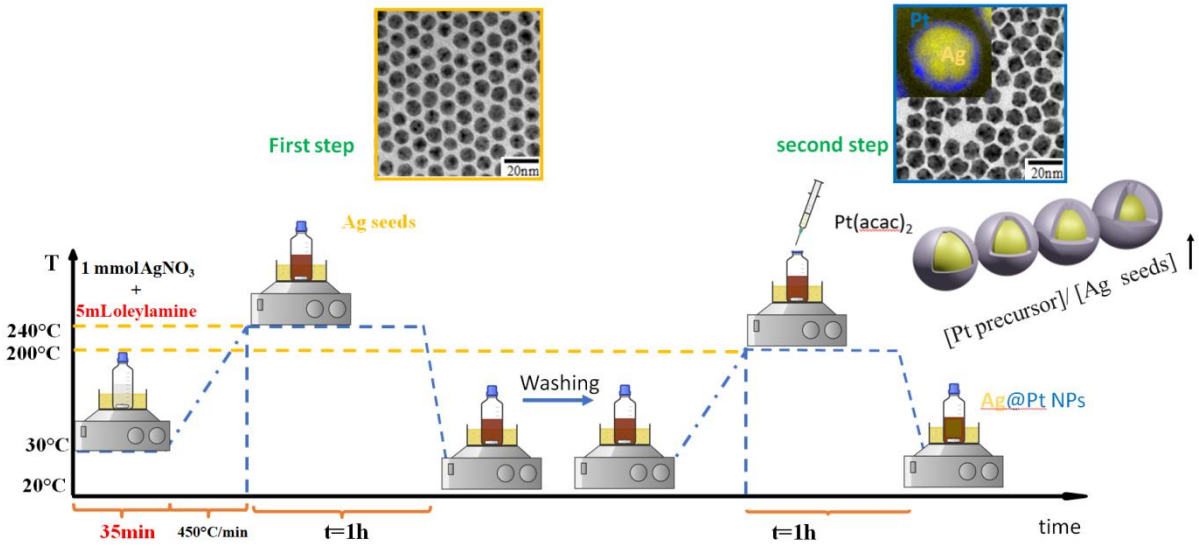

Figure 1 Representation of the two-step synthesis process for Ag@Pt NPs and exemplary TEM images of Ag and Ag@Pt NPs. Insets show corresponding EELS mapping, highlighting a silver core in yellow and a platinum shell in blue.

We have investigated the catalytic activity of our Ag@Pt core-shell NPs based on the model reaction of reduction of 4-NP to 4-AP by $NaHB_4$ in aqueous phase, which is often used to assess the performance of nanocatalysts.[21] ln chemical industries, this reaction is widely used in the fabrication of analgesics and antipyretic drugs.[22,23] The 4-NP in water has a strong absorption peak at 317 nm,[24,25] and the addition of $NaBH_4$ induces the deprotonation of OH group of 4-NP leading to the formation 4-nitrophenolate ion and a shift of absorption peak to 400 nm. The color of 4-NP solution changes thus from pale to vivid yellow due to the formation of 4-nitrophenolate ions.[26] In the presence of Ag NPs,

the color of the solution changes from vivid yellow, to light yellow and finally to transparent solution. This reaction is treated in terms of a first order reaction in the presence of $NaBH_4$ excess. The apparent reduction rate (K_{app}) is calculated from the slope of the graph $\ln(C/C_0)=f(t)$. Furthermore, temperature change does not provoke a change in mechanism in a suitable range of temperature, thus the activation energy E_a can be deduced from the respective Arrhenius plot. The model reaction of 4-NP reduction takes place in water phase while our NPs were initially synthesized in organic phase. Therefore, we transferred them into water using a previously published protocol.[18] The OLA organic ligands are exchanged MSA, which is an hydrophilic ligand. MSA has a shorter, charged ligand and allows transfer of the NPs into water and promotes adsorption of reagents onto the free surface of the NPs for catalysis. The typical images of Ag and Ag@Pt core-shell NPs before and after ligand exchange are shown Fig. 2. We observe that the NPs retain their size and shape and also a decrease of the interparticle distances that can be due to shorter chain of MSA.

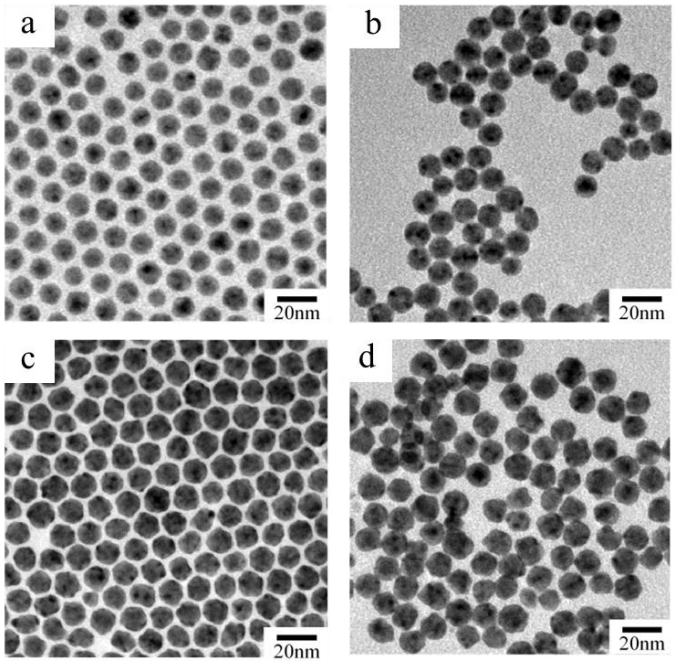

Figure 2 Typical TEM images of Ag (a, b) and Ag@Pt (c, d) NPs obtained before (a,c) and after ligand exchange (b, d).

Let us note that the catalytic activity of the nanoparticles also depends on the coverage by the ligands, i.e. the percentage of free surface accessible to the reactants. The ligands might occupy active sites, rendering them inaccessible on the surface of NPs, or hinder reactants at the NP surface due to steric hindrance [27,28]. From EDS analysis, we clearly observe after ligand exchange of oleylamine by MSA that the composition of nitrogen drops from around 19% to less than 1%, while the atomic percentage of Sulphur corresponding to MSA-protected NPs represents around 6% (see supporting information table S1). These results give evidence that oleylamine is replaced by MSA and that only a small percentage of MSA is adsorbed on the NP surface which bodes well for catalysis. We calculated the surface occupied by the MSA ligands after water transfer, and the results are presented in supporting information (section S2). We estimated an occupancy rate of 39%, assuming a binding only by the mercaptan function.

Catalytic activity of Ag core NPs. The catalytic properties of monometallic Ag NPs were investigated and compared to the bimetallic core-shell Ag@Pt system. ln the following, we will focus first on the catalytic activities of Ag NPs which were studied as a function of their size, and the results will be used as a reference to compare with the core-shell Ag@Pt NPs of similar size and different compositions. The list of NP characteristics and concentrations used for the study of their catalytic properties are summarized in SI (table S2 in SI). We monitored the reaction kinetics using UV-vis spectroscopy to follow the 4-NP to 4-AP conversion rate (see experimental section and Fig. 3a). The catalytic performances of Ag NPs with diameters of 8.4, 10.5 and 13.3 nm were evaluated from $\ln((C=[4\text{-NP}])/(C_0=[4\text{-NP}]_0))$ versus reaction time plots at 20 °C (Fig 3b). The time dependence of both the 4-NP and 4-AP absorbances for the Ag NPs with different sizes

were reported in Fig. S2 in SI. In order to consider the induction time, our fitting of the graphs ln (C/C_0) versus time plot are thus limited to the linear portion, enabling the determination of the apparent rate constant. By decreasing NP size, we observe an increase of the reduction rate constant K_{app} (see table S3). The size of the NP appears to be decisive for their catalytic activity in agreement with the literature [29,30]. The smaller the size of the NPs, the greater proportion of sub-coordinate edge and corner atoms. These edge and corner atoms are more reactive than the face atoms. We repeat the measurements for five samples and calculate the K_{app}, the measurement error from one sample to another is low (1.2%) and can be ignored. Furthermore, it shows the good reproducibility of the experiments.

We then investigated how light irradiation at the LSPR could improve the catalytic properties of our monometallic systems, as Ag NPs show the most intense plasmon of the plasmonic metals in the visible range, which makes it a potentially interesting candidate to generate hot electrons for injection in the catalytic shell.

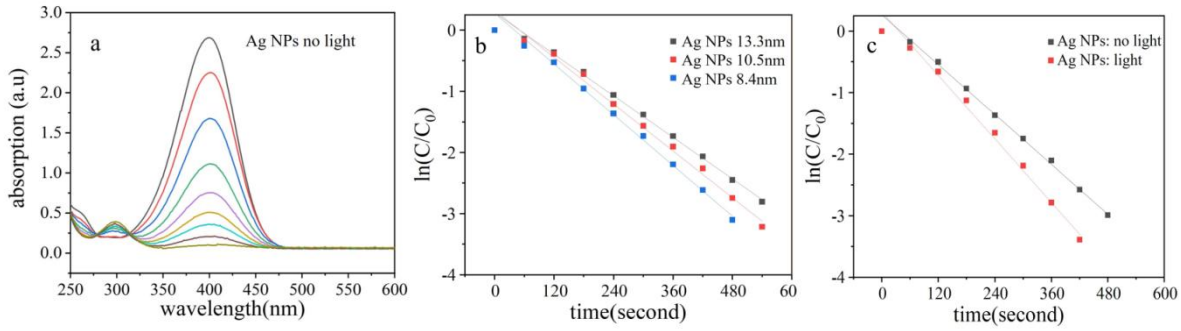

Figure 3 (a) Typical UV-visible absorption spectra obtained during the catalytic chemical reduction of 4-NP in 4-AP by Ag NP under 405 nm light irradiation, (b) corresponding plots of $\ln(C/C_0)$ versus time for the determination of rate constate for Ag NPs with diameters of 8.4, 10.5 and 13.3 nm and without NPs. (c) comparison of the apparent rate constant through the $\ln(C/C_0)$ plots versus time with and without 405 nm light irradiation during the catalysis experiment for Ag NPs with diameter of 8.4 nm

We have repeated the catalysis experiments and compared the results obtained with and without light irradiation. The light source was chosen so as to match the plasmon resonance of pure Ag NPs λ_{Laser}=405 nm at irradiance 1 Wcm^{-2} for the $Ag_{8.4nm}$ sample. The results are summarized in Fig. 3c and Table S4 in SI. Monometallic Ag showed a 22% increase in K_{app}. Light can improve catalytic reaction rates in plasmonic catalysis by several processes, namely antenna effect, local heating and hot electron generation[31], the latter two of which are related to the NP absorption and the former to the increase in photon flux at the NP due to the focusing of the electromagnetic field by the plasmonic antenna. Recently, hot electrons have been shown to promote the reduction of 4-NP to 4-AP on Ag NPs.[32] Hot electrons are produced under irradiation by non-radiative decay of Ag surface plasmons and can be transferred to molecules adsorbed on the surface, providing an additional channel for the Ag catalyzed 4-NP reduction, even in the absence of the reducing agent $NaBH_4$. However, this effect is expected to remain moderate for NPs suspended in solution for the following reasons. First hot electrons are primarily emitted at regions of intense electromagnetic field (hotspots), which are much more intense on anisotropic NPs or NPs with sharp edges. The number of hot electrons available per molecule remains limited due to high rate of charge-carrier recombination. Secondly, promoting an oxidation counter-half-reaction by photo-recycling may be necessary to balance the hot electron-induced reduction reaction, as recently demonstrated by Xie and co-workers. However the observed 22% increase of K_{app} under illumination for pure Ag is consistent with other studies which observed a 28 % increase on similar Ag NPs, and that attributed the increased reactivity to a boosting of the reactants diffusion nearby the catalyst surface due to photothermal heating.[32,33] It is not possible to disentangle the hot electron and photo-thermal contributions to the observed increased reactivity without further experiments, which is currently a major challenge in

the plasmonic catalysis community, and lies outside the scope of this work[4].

ln order to optimize the reactivity of our Ag nanocatalysts, we tested different environments rich in proton as H^+ does induce fine electrostatic interaction from the negatively charged oxygen in nitro group and facilitate the removal of oxygen and the reduction of the nitro group.[34] We have thus repeated the catalysis experiments and compared the results obtained in aqueous HCl solution under irradiation (405 nm at irradiance 1 Wcm^{-2}) with $Ag_{8.4nm}$. The results are summarized in Fig. 4a and Table 1. The Ag NPs show a 36% increase in K_{app} value in aqueous HCl solution (0.25 mM) compared to water environment. Halides were shown to play an important role in the catalyzed reduction of 4-NP to 4-AP[32]. The mechanism implying hot electrons is based on the generation of hot electron-holes pairs on Ag upon resonant excitation, combination of hot holes (h^+=Ag^+) with Cl^- ions to form photosensitive AgCl, which is further decomposed via photodissociation. Cl^- thus allow photo-recycling of the Ag surface by regenerating Ag atoms (see scheme of the mechanism in Fig. S3 in SI). In order to test if the observed increased catalytic performances were due to hot electron injection and Ag NP photorecycling by Cl^- ions, we performed the experiment in H_2SO_4 and KCl, which are respectively rich in H^+ without Cl^- and rich in Cl^- without H^+. K_{app} shows a similar increase (approximately 30%) in both HCl and H_2SO_4 (0.125 mM) without light irradiation (Fig. 4b). Under light irradiation, the Ag NPs show a 40% increase in K_{app} value in HCl and remains similar in H_2SO_4. These results show that following an additional supply of protons the conversion of 4-NP is significantly faster. This led us also the hypothesis that not only acidic conditions but also the counter anion is relevant. We tested this by adding aqueous KCl solution (0.25 mM) and repeat catalysis experiments under light source. We observed an increase of only 11% in K_{app} (Table 1).

Table 1 Evaluation of the rate conversion (K_{app}) of 4-NP using 8.4 nm Ag NPs in different environments with and without light source.

Conditions	K_{app} (10^{-3} s^{-1}) (error R^2=0.99)	K_{app} (10^{-3} s^{-1}) (error R^2=0.99)
	Under light	**Without light**
Water	8.2	6.9
HCl	11.4	9.1
H_2SO_4	10.8	9.0
KCl	9.1	-

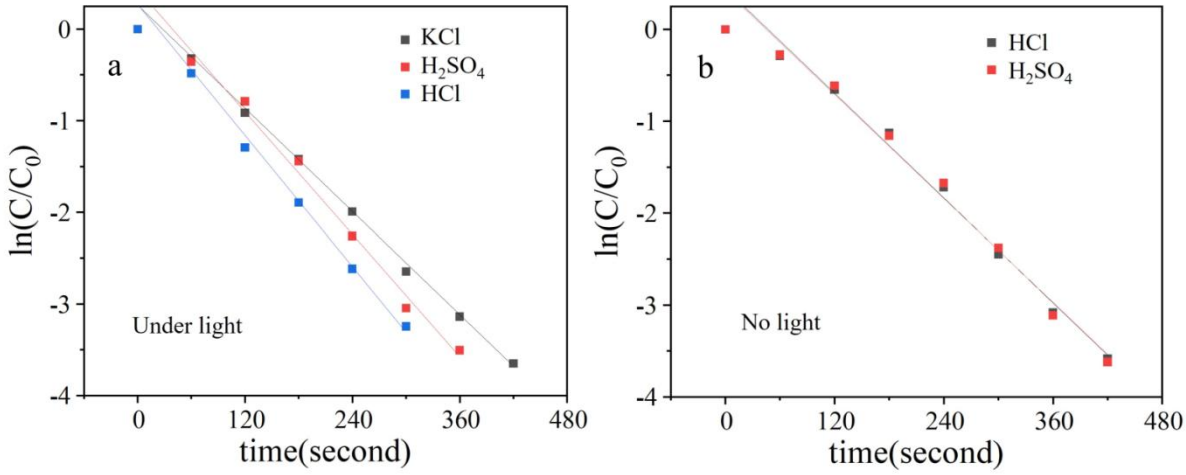

Figure 4. (a) $\ln(C/C_0)$ versus time plots for the determination of apparent rate constant for Ag NPs with diameter of 8.4 nm in presence of HCl, H_2SO_4 and KCl under 405 nm light illumination. (b) $\ln(C/C_0)$ versus time plots for the determination of apparent rate constant for Ag NPs with diameter of 8.4 nm in presence of HCl and H_2SO_4 without light illumination.

Catalytic activity from H_2SO_4 solution is thus higher than KCl, but less than HCl solution, this shows that the improvement of the catalytic activity is due to both H^+ and Cl^-. Furthermore, this indicates that Cl^- ions participate to a photo recycling mechanism

such as reported by Xie and co-workers.[32] However, the enhancement in catalytic activity due to additional H^+ does not rely on laser irradiation. To confirm the role of additional solvated protons in the reduction mechanism of 4-NP, we analyzed the variation of the apparent rate constant with H^+ (aq) concentration (Figure S4-S6 in SI). The K_{app} value demonstrates a linear increase with H^+ (aq) concentration until it reaches a plateau above a concentration of 1 mM. Considering the initial concentration of nitrophenolate is 0.15 mol L^{-1} and, in accordance with the reduction reaction, a minimum concentration of H^+ (aq) equal to 0.9 mol L^{-1} is necessary for complete reduction. The presence of a plateau at H^+ = 1 mM clearly indicates that solvated protons are the most efficient source of hydrogen.

Catalytic activity of Ag@Pt NPs. We then characterized more thoroughly the catalytic activity of our bimetallic Ag@Pt NPs with different Pt thicknesses with the same experimental conditions as Ag NPs. The bimetallic vs monometallic systems performances are summarized in the $\ln(C/C_0)$ vs time plots in Fig. 5a and 5b for Ag cores of 8.4 nm and 13.3 nm respectively.

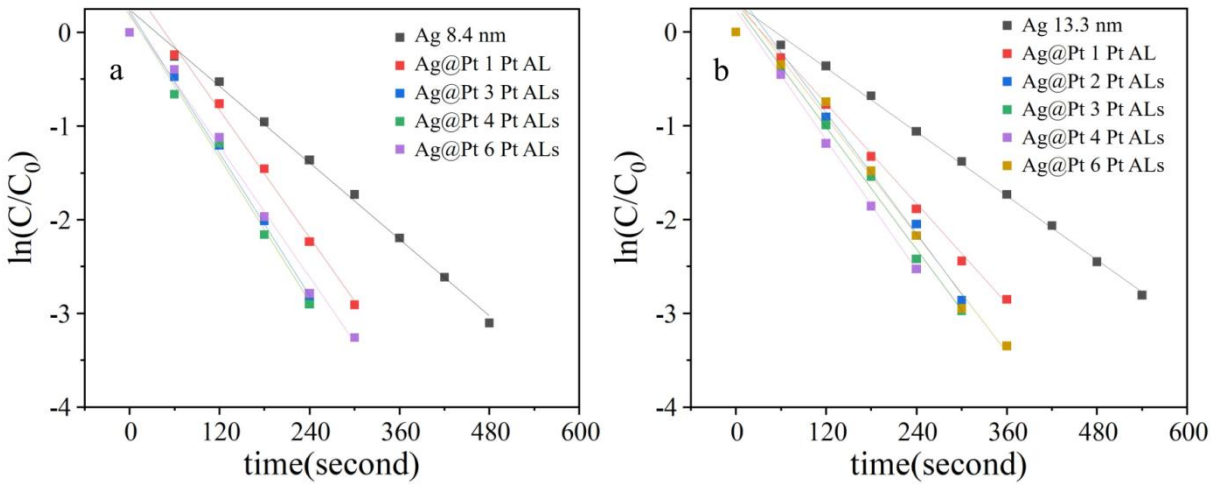

Figure 5. $\ln(C/C_0)$ versus time plots for the determination of apparent rate constant for Ag@Pt NPs with 1 - 6 Pt Atomic layers (AL) with core diameter of (a) 8.4 nm and (b) 13.3 nm**.**

The deduced K_{app} are reported in Table 2. Whatever the Ag core size, the catalytic activity of Ag@Pt increases with the Pt shell thickness. Thus, for a platinum shell thickness of e=1.1 nm (around 4 atomic layers) the K_{app} value is up to twice larger than that of the Ag seeds. Nevertheless, for a thickness of 1.7 nm, i.e. around 6 atomic layers, we observe a decrease of K_{app}. We have also tested the catalytic activity of Ag@Pt NPs for an intermediate Ag core size of 10.5 nm. We observed a similar behavior with an increase of K_{app} with the thickness of Pt shell up to a maximum number of 4 atomic layers (see Figure S7-S10 in SI and Table 2). Therefore, regardless of the core size, K_{app} increases as the Pt thickness increases up to 4 atomic layers and then decreases beyond that thickness. It decreases also with increasing core diameter (Table 2). Finally, the catalytic activity of Ag@Pt NPs remains significantly enhanced compared to pure Ag NPs, until 6 Pt layers.

Table 2: Evaluation of the rate conversion K_{app} of 4-NP using Ag and Ag@Pt NPs with different Ag sizes and Pt thicknesses.

Sample	**NP size ±0.5 nm**	**Shell thickness (nm) e ±0.3 nm**	**K_{app} (10^{-3} s^{-1}) (error R^2=0.99)**
Ag	8.4	-	6.7
Ag@Pt (8.4 nm core)	9.2	0.4 (~1 layer)	9.9
	10.1	0.85 (~3 layers)	12.1
	10.6	1.1 (~4 layers)	12.5
	12.0	1.6 (~6 layers)	11.3
Ag	10.5	-	6.1
Ag@Pt (10.5 nm core)	11.1	0.3 (~1 layer)	9.1
	11.5	0.5 (~2 layers)	9.8
	12.3	0.9 (~3 layers)	11.5
	12.7	1.1 (~4 layers)	11.6
	13.9	1.7 (~6 layers)	10.9
Ag	13.3	-	5.4
Ag@Pt (13.3 nm core)	13.8	0.3 (~1 layer)	8.3
	14.2	0.5 (~2 layers)	9.5

	15.1	0.9 (~3 layers)	10.5
	15.5	1.1 (~4 layers)	10.7
	16.5	1.7 (~6 layers)	10.0

Pt catalytic activity is controlled by its electronic structure through its d-band center, which is sensitive to lattice strain. ln the case of core-shell bimetallic nanocatalysts, the core and shell lattice mismatch can lead to strain which in turn can modify the adsorption energy of the adsorbate. This effect has been observed before in various reactions on metal core - Pt shell nanocatalysts and can vary depending on whether the mismatch induces a compressive or a tensile strain in the outer Pt shell.[35–37]. The former and the latter induce respectively a downshift or an upshift of the d band centers. Upshifts tend to push the antibonding metal d adsorbate states above the Fermi level, which makes the Pt (d) ~ adsorbate interaction more attractive.[3,38] Here with Ag@Pt core-shell NPs, Ag core has a larger lattice parameter and thus induces a tensile strain in the Pt shell, yielding a Pt d-band center upshift away from the Fermi level, anti-bonding orbitals depopulation and a stronger interaction of 4-NP with the Pt surface. Enhanced chemisorption is not generally reported to improve the catalytic activity of the Pt shell [39]. However, with increased Pt shell (more than 4 atomic layers) that induces a decrease of the tensile-strain, the catalytic activity is observed to decrease.

Looking at the electronic structure of Ag@Pt core-shell NPs can explain their increased reactivity compared to pure Ag NPs. DFT calculations have shown that in Ag@Pt core-shell NPs, electrons accumulate in the Pt region, and Pt atomic population become more negatively charged compared to Ag core subsequent to Pt coating, indicating a charge transfer from Ag to Pt layers.[40] This is associated with a strong (Ag)s-(Pt)d hybridization at the origin of the charge redistribution between Ag cores and Pt shells. The increased electron density in the Pt layer makes more electrons available for the 4-NP reduction at the surface and can explain the improvement of the Ag@Pt catalytic performance

compared to pure Ag. When the Pt layer becomes too thick, above 4 monolayers, we can assume that the ligand effects (electronic transfer) is deteriorated and a decrease of the reactivity of NPs is observed.[41].

Light irradiation effects on catalytic activity of Ag@Pt NPs. We have repeated the catalysis experiments for $Ag_{8.4nm}$@Pt with 1 Pt atomic layer and 4 Pt atomic layers with light irradiation (λ=405 nm at irradiance 1 W cm^{-2}). Core-shell Ag@Pt 1 Pt layer showed a slight 5% increase in K_{app} value (Fig. S11), while Ag@Pt 4 Pt layers showed no catalytic improvement upon light irradiation (see Table S4). The low light harvesting of Ag@Pt core-shell NPs can be attributed to a damping of the Ag LSPR as soon as the first Pt layer grows in line with our previous study.[18] Furthermore, our results are supported by a recent article demonstrating that hot electrons transfer across a Pt shell from an Au core depend on the shell thickness because according with DFT calculations, hot electrons can only travel a very short distance in metals (<1 nm)[42]. Thus to compensate for the low light harvesting of dispersed Ag@Pt NPs, we have considered in a recently published paper [43]their 3D organization into colloidal supercrystals (SCs) in order to promote coupling between the NPs and an enhancement of the local electromagnetic field, which strongly depends on the inter-NP distance, and which leads to the creation of hot spot accelerating the generation of localized hot electrons. We got evidence of plasmonic photo catalytic activity of supported Ag@Pt SCs, particularly in the context of Hydrogen evolution reaction (HER)[43].

Temperature Effect on catalytic activity of Ag and Ag@Pt NPs. We carried out a series of reaction for the reduction of 4-NP to 4-AP in the presence of Ag or Ag@Pt NPs for a fixed Ag core diameter of 8.4 nm, in order to determine how the temperature can affect the kinetics of this reaction. The apparent rate constants K_{app} obtained for different reaction temperatures between 20 and 40°C are summarized in Table S5 in SI. Based on

Arrhenius equation:

$$k = -Ae^{-E_a/RT} \text{ (equation 2)}$$

where A is the frequency factor, E_a is the activation energy, R is the thermodynamic gas constant, and T is the circumstance temperature. By plotting the graph of apparent rate constant K_{app} for each catalytic system versus corresponding 1/T one can obtain the activation energy (E_a, apparent) for the reduction of 4-NP for each catalytic system (Figure 6a). The minimum of activation energy is observed for $Ag_{8.4nm}$@Pt NPs with a thickness corresponding to 4 atomic layers (Figure 6b). The apparent activation energy (E_a) is calculated to be around 10.3 $kJ.mol^{-1}$, which is much lower than those reported for Ag or Pt based catalysts[19] and further illustrates the synergistic catalytic effect of Ag and Pt species. Finally, the Ag@Pt NPs with the smallest core size led to the minimal activation energy and present thus the higher reactivity.

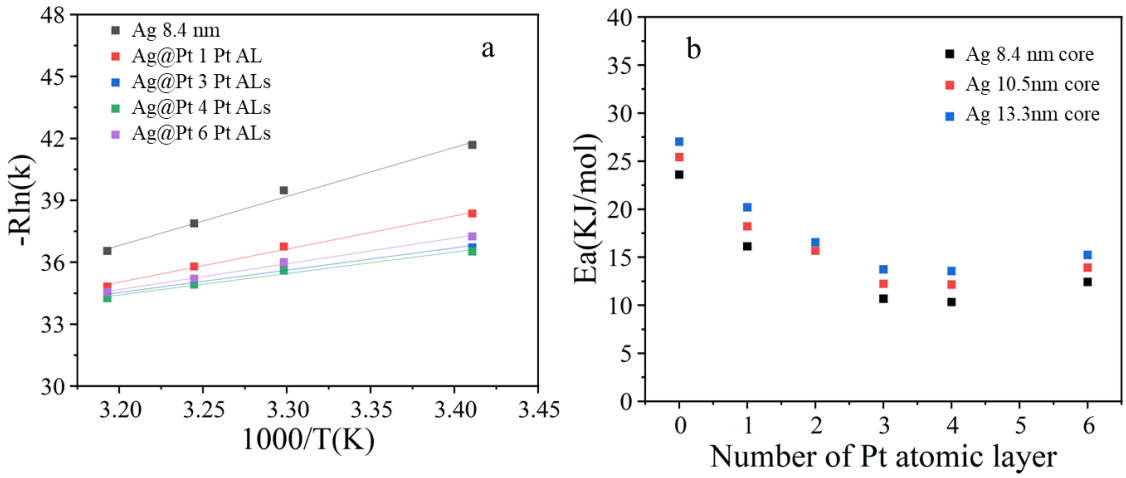

Figure 6. (a) Linear fitting of -Rln(k)=f(1000/T(K)) for Ag and Ag@Pt NPs with a core of 8.4 nm in diameter and with 1-6 Pt atomic Layers (AL) and (b) corresponding activation energies.

Recyclability of Ag@Pt nanocatalysts. The recycling of the NP catalyst has become an important point, especially for economic reason. The reusability of NPs was thus investigated in the reduction of 4-NP. Ag@Pt NPs with Ag core diameter of 8.4 nm and 4 Pt atomic layers were reused to carry out the reduction process for 3 consecutive runs. The value of K_{app} for each catalytic reaction run was calculated from plots of ln (C/C_0) versus time deduced from the UV-visible absorption spectra (Fig. S12). The rate constants for successive cycles are shown in Table S6. The obtained results for these cycles show a very slight diminution (2%) of K_{app} which emphasizes the high activity of the NPs and their good stability.

3. Conclusions

The catalytic activity of core-shell Ag and Ag@Pt nanoparticles was investigated using the model reaction of 4-nitrophenol reduction to 4-aminophenol. Initially, we examined the catalytic performance of pure Ag nanoparticles of varying sizes and found that those with smaller diameters exhibited the highest activity. Additionally, the introduction of aqueous solutions of HCl or H_2SO_4 was found to enhance the catalytic conversion rate by introducing H^+ ions. Furthermore, under light irradiation, the presence of a halide further increased the catalytic efficiency of Ag nanoparticles through a mechanism of photo-recycling and hot electron generation.

Subsequently, we demonstrated that the catalytic properties of Ag@Pt nanoparticles are influenced by the thickness of the Pt shell and the size of the Ag core. Specifically, optimal catalytic activity was achieved when the Pt shell thickness reached a maximum of four atomic layers, accompanied by a reduction in the size of the Ag core for a fixed Pt shell thickness. The catalytic activity of Ag@Pt nanoparticles surpassed that of monometallic Ag nanoparticles of comparable core size. Light irradiation was shown to

marginally increase their catalytic activity, attributed to an attenuated plasmonic effect and/or inhibition of hot electron transfer to molecular reactants by the one-atomic-layer Pt shell.

Finally, Ag@Pt nanoparticles exhibited good stability and could be reused without significant loss of activity after three recycling cycles.

Our study thus enhances our understanding of the complex relationship between the structure and activity of bimetallic nanoparticles. Core size and shell thickness emerge as important parameters for controlling the catalytic activity of bimetallic core-shell nanoparticles.

ASSOCIATED CONTENT

Supporting Information. The following files are available free of charge. Additional data on the catalytic performance of Ag and Ag@Pt NPs for the reduction of 4-NP to 4-AP in the form of tables, UV-visible absorption spectra or data processing graphs.

Author Contribution

The manuscript was written through contributions of all authors. All authors have given approval to the final version of the manuscript**.**

ACKNOWLEDGMENT

The authors thank the Chinese Scholarship Council for the thesis grant. AC, CS and AG thank Sorbonne University and the CNRS for facilities. This work was supported by the ANR PlLOT project, grant ANR-20-CE09-0006 of the French Agence Nationale de la Recherche.

References:

(1) Loza, K.; Heggen, M.; Epple, M. Synthesis, Structure, Properties, and Applications of Bimetallic Nanoparticles of Noble Metals. *Adv. Funct. Mater.* **2020**, *30* (21), 1909260.

https://doi.org/10.1002/adfm.201909260.
(2) Araujo, T. P.; Quiroz, J.; Barbosa, E. C. M.; Camargo, P. H. C. Understanding Plasmonic Catalysis with Controlled Nanomaterials Based on Catalytic and Plasmonic Metals. *Curr. Opin. Colloid Interface Sci.* **2019**, *39*, 110–122. https://doi.org/10.1016/j.cocis.2019.01.014.
(3) Sytwu, K.; Vadai, M.; Dionne, J. A. Bimetallic Nanostructures: Combining Plasmonic and Catalytic Metals for Photocatalysis. *Adv. Phys. X* **2019**, *4* (1). https://doi.org/10.1080/23746149.2019.1619480.
(4) Zhan, C.; Yi, J.; Hu, S.; Zhang, X.-G.; Wu, D.-Y.; Tian, Z.-Q. Plasmon-Mediated Chemical Reactions. *Nat. Rev. Methods Primer* **2023**, *3* (1), 12. https://doi.org/10.1038/s43586-023-00195-1.
(5) Zhang, C.; Kong, T.; Fu, Z.; Zhang, Z.; Zheng, H. Hot Electron and Thermal Effects in Plasmonic Catalysis of Nanocrystal Transformation. *Nanoscale* **2020**, *12* (16), 8768–8774. https://doi.org/10.1039/c9nr10041e.
(6) Kim, M.; Lin, M.; Son, J.; Xu, H.; Nam, J. M. Hot-Electron-Mediated Photochemical Reactions: Principles, Recent Advances, and Challenges. *Adv. Opt. Mater.* **2017**, *5* (15), 1–21. https://doi.org/10.1002/adom.201700004.
(7) Zhang, Y.; He, S.; Guo, W.; Hu, Y.; Huang, J.; Mulcahy, J. R.; Wei, W. D. Surface-Plasmon-Driven Hot Electron Photochemistry. *Chem. Rev.* **2018**, *118* (6), 2927–2954. https://doi.org/10.1021/acs.chemrev.7b00430.
(8) Kim, Y.; Dumett Torres, D.; Jain, P. K. Activation Energies of Plasmonic Catalysts. *Nano Lett.* **2016**, *16* (5), 3399–3407. https://doi.org/10.1021/acs.nanolett.6b01373.
(9) Zhou, L.; Lou, M.; Bao, J. L.; Zhang, C.; Liu, J. G.; Martirez, J. M. P.; Tian, S.; Yuan, L.; Swearer, D. F.; Robatjazi, H.; Carter, E. A.; Nordlander, P.; Halas, N. J. Hot Carrier Multiplication in Plasmonic Photocatalysis. *Proc. Natl. Acad. Sci. U. S. A.* **2021**, *118* (20), 1–6. https://doi.org/10.1073/pnas.2022109118.
(10) Lin, S.-C.; Hsu, C.-S.; Chiu, S.-Y.; Liao, T.-Y.; Chen, H. M. Edgeless Ag–Pt Bimetallic Nanocages: In Situ Monitor Plasmon-Induced Suppression of Hydrogen Peroxide Formation. *J. Am. Chem. Soc.* **2017**, *139* (6), 2224–2233. https://doi.org/10.1021/jacs.6b09080.
(11) Swearer, D. F.; Zhao, H.; Zhou, L.; Zhang, C.; Robatjazi, H.; Martirez, J. M. P.; Krauter, C. M.; Yazdi, S.; McClain, M. J.; Ringe, E.; Carter, E. A.; Nordlander, P.; Halas, N. J. Heterometallic Antenna-Reactor Complexes for Photocatalysis. *Proc. Natl. Acad. Sci. U. S. A.* **2016**, *113* (32), 8916–8920. https://doi.org/10.1073/pnas.1609769113.
(12) Guo, J.; Zhang, Y.; Shi, L.; Zhu, Y.; Mideksa, M. F.; Hou, K.; Zhao, W.; Wang, D.; Zhao, M.; Zhang, X.; Lv, J.; Zhang, J.; Wang, X.; Tang, Z. Boosting Hot Electrons in Hetero-Superstructures for Plasmon-Enhanced Catalysis. *J. Am. Chem. Soc.* **2017**, *139* (49), 17964–17972. https://doi.org/10.1021/jacs.7b08903.
(13) Wu, X.; Zhu, X.; Kan, C.; Shi, D. Bimetallic Au@Rh Core–Shell Nanostars with Plasmon-Enhanced Catalytic Performance in Hydrogen Evolution Reaction. *CrystEngComm* **2023**, *25* (9), 1365–1373. https://doi.org/10.1039/D2CE01630C.
(14) Vadai, M.; Angell, D. K.; Hayee, F.; Sytwu, K.; Dionne, J. A. In-Situ Observation of Plasmon-Controlled Photocatalytic Dehydrogenation of Individual Palladium Nanoparticles. *Nat. Commun.* **2018**, *9* (1), 1–8. https://doi.org/10.1038/s41467-018-07108-x.
(15) Zaleska-Medynska, A.; Marchelek, M.; Diak, M.; Grabowska, E. Noble Metal-Based Bimetallic Nanoparticles: The Effect of the Structure on the Optical, Catalytic and Photocatalytic Properties. *Adv. Colloid Interface Sci.* **2016**, *229*, 80–107. https://doi.org/10.1016/j.cis.2015.12.008.
(16) Eom, N.; Messing, M. E.; Johansson, J.; Deppert, K. General Trends in Core–Shell Preferences for Bimetallic Nanoparticles. *ACS Nano* **2021**, *15* (5), 8883–8895. https://doi.org/10.1021/acsnano.1c01500.
(17) Zhang, Y.-J.; Li, S.-B.; Duan, S.; Lu, B.-A.; Yang, J.; Panneerselvam, R.; Li, C.-Y.; Fang, P.-P.; Zhou, Z.-Y.; Phillips, D. L.; Li, J.-F.; Tian, Z.-Q. Probing the Electronic Structure of Heterogeneous Metal Interfaces by Transition Metal Shelled Gold Nanoparticle-Enhanced Raman Spectroscopy. *J. Phys. Chem. C* **2016**, *120* (37), 20684–20691. https://doi.org/10.1021/acs.jpcc.6b01879.
(18) Fan, Y.; Girard, A.; Waals, M.; Salzemann, C.; Courty, A. Ag@Pt Core–Shell Nanoparticles for Plasmonic Catalysis. *ACS Appl. Nano Mater.* **2023**, *6* (2), 1193–1202.

https://doi.org/10.1021/acsanm.2c04767.
(19) Jiang, H.-L.; Akita, T.; Ishida, T.; Haruta, M.; Xu, Q. Synergistic Catalysis of AuAg Core Shell Nanoparticles Stabilized on Metal Organic Framework. *J. Am. Chem. Soc.* **2011**, *133* (5), 1304–1306. https://doi.org/10.1021/ja1099006.
(20) Mares-Briones, F.; Barragán-Mares, O.; López-Miranda, J. L.; Esparza, R.; Rosas, G. Bimetallic Ag@Pt Core-Shell Nanoparticles and Their Catalytic Activity by a Green Approach. *Mater. Res. Express* **2019**, *6* (8), 0850h8. https://doi.org/10.1088/2053-1591/ab299c.
(21) Wang, Z.; Xu, C.; Gao, G.; Li, X. Facile Synthesis of Well-Dispersed Pd–Graphene Nanohybrids and Their Catalytic Properties in 4-Nitrophenol Reduction. *RSC Adv.* **2014**, *4* (26), 13644. https://doi.org/10.1039/c3ra47721e.
(22) Berahim, N.; Basirun, W.; Leo, B.; Johan, M. Synthesis of Bimetallic Gold-Silver (Au-Ag) Nanoparticles for the Catalytic Reduction of 4-Nitrophenol to 4-Aminophenol. *Catalysts* **2018**, *8* (10), 412. https://doi.org/10.3390/catal8100412.
(23) Arora, N.; Mehta, A.; Mishra, A.; Basu, S. 4-Nitrophenol Reduction Catalysed by Au-Ag Bimetallic Nanoparticles Supported on LDH: Homogeneous vs. Heterogeneous Catalysis. *Appl. Clay Sci.* **2018**, *151*, 1–9. https://doi.org/10.1016/j.clay.2017.10.015.
(24) Haldar, K. K.; Kundu, S.; Patra, A. Core-Size-Dependent Catalytic Properties of Bimetallic Au/Ag Core–Shell Nanoparticles. *ACS Appl. Mater. Interfaces* **2014**, *6* (24), 21946–21953. https://doi.org/10.1021/am507391d.
(25) Ahmed Zelekew, O.; Kuo, D.-H. A Two-Oxide Nanodiode System Made of Double-Layered p-Type Ag_2O@n-Type TiO_2 for Rapid Reduction of 4-Nitrophenol. *Phys. Chem. Chem. Phys.* **2016**, *18* (6), 4405–4414. https://doi.org/10.1039/C5CP07320K.
(26) Krishnamurthy, S.; Esterle, A.; Sharma, N. C.; Sahi, S. V. Yucca-Derived Synthesis of Gold Nanomaterial and Their Catalytic Potential. *Nanoscale Res. Lett.* **2014**, *9* (1), 627. https://doi.org/10.1186/1556-276X-9-627.
(27) Neal, R. D.; Inoue, Y.; Hughes, R. A.; Neretina, S. Catalytic Reduction of 4-Nitrophenol by Gold Catalysts: The Influence of Borohydride Concentration on the Induction Time. *J. Phys. Chem. C* **2019**, *123* (20), 12894–12901. https://doi.org/10.1021/acs.jpcc.9b02396.
(28) Ansar, S. M.; Kitchens, C. L. Impact of Gold Nanoparticle Stabilizing Ligands on the Colloidal Catalytic Reduction of 4-Nitrophenol. *ACS Catal.* **2016**, *6* (8), 5553–5560. https://doi.org/10.1021/acscatal.6b00635.
(29) Zhou, X.; Xu, W.; Liu, G.; Panda, D.; Chen, P. Size-Dependent Catalytic Activity and Dynamics of Gold Nanoparticles at the Single-Molecule Level. *J. Am. Chem. Soc.* **2010**, *132* (1), 138–146. https://doi.org/10.1021/ja904307n.
(30) Isaifan, R. J.; Ntais, S.; Baranova, E. A. Particle Size Effect on Catalytic Activity of Carbon-Supported Pt Nanoparticles for Complete Ethylene Oxidation. *Appl. Catal. Gen.* **2013**, *464–465*, 87–94. https://doi.org/10.1016/j.apcata.2013.05.027.
(31) Baffou, G.; Quidant, R. Nanoplasmonics for Chemistry. *Chem. Soc. Rev.* **2014**, *43* (11), 3898–3907. https://doi.org/10.1039/c3cs60364d.
(32) Xie, W.; Schlücker, S. Hot Electron-Induced Reduction of Small Molecules on Photorecycling Metal Surfaces. *Nat. Commun.* **2015**, *6* (July). https://doi.org/10.1038/ncomms8570.
(33) Gao, S.; Zhang, Z.; Liu, K.; Dong, B. Direct Evidence of Plasmonic Enhancement on Catalytic Reduction of 4-Nitrophenol over Silver Nanoparticles Supported on Flexible Fibrous Networks. *Appl. Catal. B Environ.* **2016**, *188*, 245–252. https://doi.org/10.1016/j.apcatb.2016.01.074.
(34) Kong, X.; Zhu, H.; Chen, C.; Huang, G.; Chen, Q. Insights into the Reduction of 4-Nitrophenol to 4-Aminophenol on Catalysts. *Chem. Phys. Lett.* **2017**, *684*, 148–152. https://doi.org/10.1016/j.cplett.2017.06.049.
(35) Bu, L.; Zhang, N.; Guo, S.; Zhang, X.; Li, J.; Yao, J.; Wu, T.; Lu, G.; Ma, J.-Y.; Su, D.; Huang, X. Biaxially Strained PtPb/Pt Core/Shell Nanoplate Boosts Oxygen Reduction Catalysis. *Science* **2016**, *354* (6318), 1410–1414. https://doi.org/10.1126/science.aah6133.
(36) Strasser, P.; Koh, S.; Anniyev, T.; Greeley, J.; More, K.; Yu, C.; Liu, Z.; Kaya, S.; Nordlund, D.; Ogasawara, H.; Toney, M. F.; Nilsson, A. Lattice-Strain Control of the Activity in Dealloyed Core-Shell Fuel Cell Catalysts. *Nat. Chem.* **2010**, *2* (6), 454–460. https://doi.org/10.1038/nchem.623.
(37) van der Hoeven, J. E. S.; Jelic, J.; Olthof, L. A.; Totarella, G.; van Dijk-Moes, R. J. A.; Krafft, J.

M.; Louis, C.; Studt, F.; van Blaaderen, A.; de Jongh, P. E. Unlocking Synergy in Bimetallic Catalysts by Core–Shell Design. *Nat. Mater.* **2021**, *20* (9), 1216–1220. https://doi.org/10.1038/s41563-021-00996-3.
(38) Hammer, B.; Nørskov, J. K. Theoretical Surface Science and Catalysis—Calculations and Concepts. *Adv. Catal.* **2000**, *45* (C), 71–129. https://doi.org/10.1016/S0360-0564(02)45013-4.
(39) Wu, J.; Li, P.; Pan, Y.-T. (Frank); Warren, S.; Yin, X.; Yang, H. Surface Lattice-Engineered Bimetallic Nanoparticles and Their Catalytic Properties. *Chem. Soc. Rev.* **2012**, *41* (24), 8066. https://doi.org/10.1039/c2cs35189g.
(40) Ma, Y.; Wu, X.; Zhang, G. Core-Shell Ag@Pt Nanoparticles Supported on Sepiolite Nanofibers for the Catalytic Reduction of Nitrophenols in Water: Enhanced Catalytic Performance and DFT Study. *Appl. Catal. B Environ.* **2017**, *205*, 262–270. https://doi.org/10.1016/j.apcatb.2016.12.025.
(41) Gao, F.; Goodman, D. W. Pd–Au Bimetallic Catalysts: Understanding Alloy Effects from Planar Models and (Supported) Nanoparticles. *Chem. Soc. Rev.* **2012**, *41* (24), 8009. https://doi.org/10.1039/c2cs35160a.
(42) Zhang, H.; Wei, J.; Zhang, X.-G.; Zhang, Y.-J.; Radjenovica, P. M.; Wu, D.-Y.; Pan, F.; Tian, Z.-Q.; Li, J.-F. Plasmon-Induced Interfacial Hot-Electron Transfer Directly Probed by Raman Spectroscopy. *Chem* **2020**, *6* (3), 689–702. https://doi.org/10.1016/j.chempr.2019.12.015.
(43) Fan, Y.; Walls, M.; Salzemann, C.; Noël, J.; Kanoufi, F.; Courty, A.; Lemineur, J. Metal Core–Shell Nanoparticle Supercrystals: From Photoactivation of Hydrogen Evolution to Photocorrosion. *Adv. Mater.* **2023**, *35* (45), 2305402. https://doi.org/10.1002/adma.202305402.

SYNOPSIS

Optimal conditions for the catalytic reduction of 4-nitrophenol in 4-aminophenol using Ag or Ag@Pt nanocatalysts.

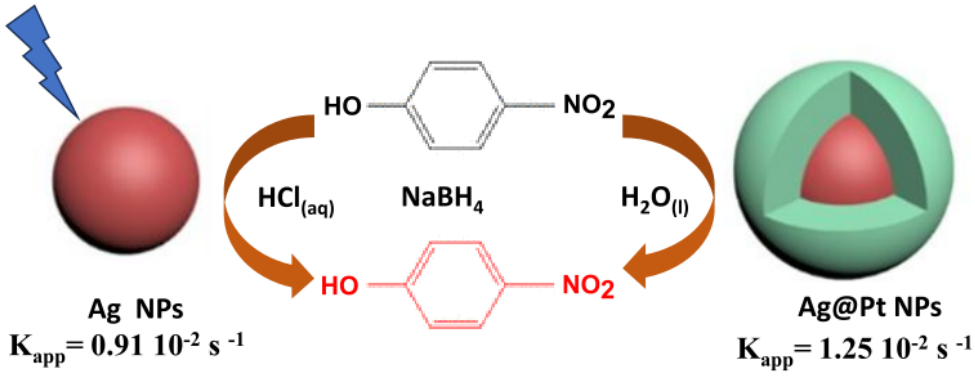
HO
NO2
HCl(aq)
NaBH4
H2O(l)
HO
NO2
Ag NPs
Kapp= 0.91 10-2 s -1
Ag@Pt NPs
Kapp= 1.25 10-2 s -1